Micron 42 (2011) 456–460

Contents lists available at ScienceDirect

Micron

journal homepage: www.elsevier.com/locate/micron

EMCD real space maps of *Magnetospirillum magnetotacticum*

M. Stöger-Pollach[a,*], C.D. Treiber[b], G.P. Resch[b,c], D.A. Keays[b], I. Ennen[d]

[a] University Service Center for Transmission Electron Microscopy, Technische Universität Wien, Wiedner Hauptstraße 8-10, A-1040 Wien, Austria
[b] Research Institute of Molecular Pathology, Dr. Bohr-Gasse 7, A-1030 Wien, Austria
[c] Institute of Molecular Biotechnology, Dr. Bohr-Gasse 3, A-1030 Wien, Austria
[d] Institute for Solid State Physics, Technische Universität Wien, Wiedner Hauptstraße 8-10, A-1040 Wien, Austria

ARTICLE INFO

Article history:
Received 7 September 2010
Received in revised form 12 January 2011
Accepted 15 January 2011

Keywords:
TEM
Magnetic circular dichroism
Magnetotactic bacteria
Biogenic magnetite
Mapping of magnetic properties

ABSTRACT

In this study we combine energy loss magnetic circular dichroism (EMCD) and energy filtered transmission electron microscopy (EFTEM) to map magnetic properties of nanoparticles. We show that it is a functional tool for investigating the magnetic behaviour of bio-mineralized magnetite crystals of *Magnetospirillum magnetotacticum*. We find that the spatial resolution of our experimental set-up is in the range of less than 2 nm. The results are compared with EMCD studies of abiogenic magnetite.

1. Introduction

The mapping of magnetic properties on a nanometer scale is a major challenge. This field was pioneered by using X-ray absorption spectroscopy (XAS) leading to a technique known as X-ray magnetic circular dichroism (XMCD). Recently Lam et al. (2010) succeeded in characterizing the magnetic properties of individual bio-mineralized magnetite particles by using XMCD in a scanning transmission X-ray microscope (STXM). In the STXM the X-rays are focused to a point and the sample is mechanically scanned through the produced focal spot. At each point the transmitted X-rays are recorded. The availability of such apparatus is limited, because a synchrotron is needed to generate X-rays that are sufficiently bright. Moreover, in XMCD there is a limitation with respect to the spatial resolution because X-ray lenses are difficult to produce. Only the recent development of Fresnel-lenses for X-rays has enabled XMCD investigators to achieve a spatial resolution of up to 20 nm.

The mathematical descriptions of XAS and electron energy loss spectrometry (EELS) show many parallels. It was only a matter of time until the analogue to XMCD was found for electrons. For XAS the inelastic scattering cross section σ is

$$\sigma = 2\pi h\alpha\omega \sum_{i,f} |\langle i|\vec{e}\hat{R}|f\rangle|^2 \delta(E + E_i - E_f) \quad (1)$$

with i, f as the initial and final states, h as Planck's constant, ω as the frequency of the X-ray, α as the fine structure constant, $\vec{e}$ as the polarization vector of the circularly polarized X-ray, $\hat{R}$ as the space operator and $\delta(E + E_i - E_f)$ as the absorbed energy. For inelastic electron scattering the double differential scattering cross section $\partial^2\sigma/\partial E\partial\Omega$ is proportional to the dynamic form factor (DFF) (Kohl and Rose, 1985) which is

$$\mathrm{DFF} = \sum_{i,f} |\langle i|\vec{q}\hat{R}|f\rangle|^2 \delta(E + E_i - E_f) \quad (2)$$

with $\vec{q}$ as the momentum transfer. These similarities recognized by Hébert and Schattschneider (2003) led to the invention of a method known as energy loss magnetic chiral dichroism (EMCD) (Schattschneider et al., 2006). In parallel with the experimental progress the theory for spin dependent EMCD *ab initio* simulations has been developed. This development has allowed the formulation of EMCD sum rules comparable to those valid for XMCD (Rusz et al., 2008).

Hand-in-hand with these simulations the experimental methods are also improving, to the point where nanometer scale analysis of magnetic properties is now possible. Although the ultimate goal of imaging electron orbits of magnetic systems has not yet been reached, recent studies have achieved a spatial resolution of less than 2 nm in EMCD analysis on an Fe/Au multilayer stack (Schattschneider et al., 2008). In that work specimen drift limited the EMCD mapping to line scans only. However, for stable specimens or with an ad hoc drift correction procedure the chiral scanning TEM (STEM) method could be employed to obtain EMCD maps similar to the spectrum imaging method proposed

* Corresponding author.
E-mail address: stoeger@ustem.tuwien.ac.at (M. Stöger-Pollach).

0968-4328/$ – see front matter © 2011 Elsevier Ltd. All rights reserved.
doi:10.1016/j.micron.2011.01.003

by Jeanguillaume and Colliex (1989). Such high spatial resolution can be achieved in the transmission electron microscope (TEM) in two ways, either in the scanning mode or in the imaging mode. The scanning mode has a few advantages over the conventional imaging mode. The obvious advantage is that STEM permits two extra signals on top of the EMCD signal in the same experiment. These two additional signals are characteristic X-rays (that can be processed in energy dispersive X-ray analysis) and elastic large angle electron scattering (that is used for Z-contrast imaging with a high angle annular dark field detector; see for example: Batson (1992)). Modern machines have both operation modes, TEM and STEM (S-TEM). Recent developments of S-TEMs have corrected lens systems, that compensate for spherical aberrations in the condenser system (probe C_s corrector) (Krivanek et al., 1999) and in the objective lens system (image C_s corrector) (Rose, 1999). This development can further improve the spatial resolution of STEM-EMCD, however, the primary limitation is that only small areas can be probed within a reasonable time. To overcome this drawback one approach is to employ EMCD-energy filtered TEM (EMCD-EFTEM) maps (Hébert et al., 2008). To date however, this has only been successfully applied to an iron single crystal by Lidbaum et al. (2010).

Here we perform EMCD-EFTEM on magnetite particles in magnetotactic bacteria, *Magnetospirillum magnetotacticum*, directly mapping their magnetic footprint on a nm-scale. These bipolar flagellated gram-negative bacteria were first isolated and described by Blakemore (1975), who showed that the bacteria's motility is directed by magnetic fields. The bacteria orient along magnetic field lines with the help of a specialized organelle that consists of small magnetite ($Fe_2^{3+}Fe^{2+}O_4$) crystals (Frankel et al., 1979), enveloped by a phospholipid bilayer (Gorby and Beveridge, 1988). These particles are organized in straight chains and produce an overall magnetic dipole moment (Dunin-Borkowski et al., 1998).

We demonstrate that EMCD-EFTEM is a reliable tool for measuring the circular magnetic dichroism on an area more amenable to experimental investigation without loosing spatial resolution.

2. Materials and methods

M. magnetotacticum strain MS-1 (Maratea and Blakemore, 1981) was acquired from DSMZ, Braunschweig, Germany. The bacteria were concentrated from the stock solution in 1.5 ml Eppendorf tubes on an Invitrogen DynaMag spin magnet. For negative staining, 20 μl of concentrated bacteria were pipetted onto a carbon-coated 400 mesh Cu grid, adsorbed for a minute and negatively stained with two exchanges of 2% aqueous uranyl acetate, to increase the visibility of the biological specimen.

For the EMCD maps a conventional TECNAI F20 TEM equipped with a field emission gun and a GATAN GIF Tridiem energy loss filter and spectrometer was used. It was operated at 200 kV acceleration voltage for the electron probe.

Inelastic dark field images were recorded by using inelastically scattered electrons having undergone the ionization process for iron L-edges from a rather low intensity area of the diffraction pattern which is the Thales position as described by Schattschneider et al. (2006). The energy loss near edge structure (ELNES) of the iron $L_{2,3}$-edges is due to the $2p_{3/2}$ and $2p_{1/2}$ to vacuum transitions with an ionization energy of 709 eV and 721 eV, respectively. The EMCD signal (which is the difference between the two ELNES spectra) shows a strong thickness dependency (Rusz et al., 2007). The general tendency shows a decreasing dichroic effect with increasing sample thickness. This trend is modulated by the *pendellösung* of both the incoming and outgoing wave functions as described by Löffler and Schattschneider (2010). Therefore relatively thin samples have to be studied. In this study the magnetite crystals have

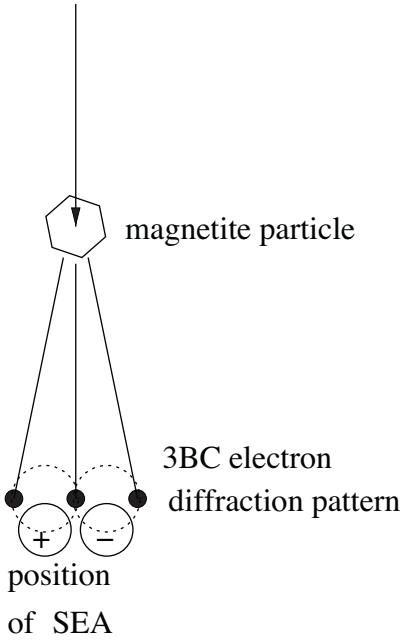

Fig. 1. Experimental set-up for EMCD spectroscopy and EMCD imaging. In the case of EMCD imaging, the objective aperture (OA) takes the role of the spectrometer entrance aperture (SEA), which is used for spectroscopy.

a dimension of only 32 nm. Hence, the ionization cross-section is also very small.

For calculating the required exposure time of an elemental map with the objective aperture (OA) on the Thales circle position one has to consider the Lorentzian distribution of the Fe-L edge in the reciprocal plane. The intensity decreases by one order of magnitude compared to the undiffracted spot. The dynamic range from the elastic peak to the Fe-L_3 signal is extreme for such thin samples. This is demonstrated in Fig. 2. The elastic peak contains seven orders of magnitude more intensity than the iron signal after back ground subtraction. Hence, the total intensity ratio of the elastic peak and the Fe-L_3 edge recorded in the chiral position is approximately 10^8. As soon as the elastic image of the bacterium is recorded, it is straight forward to calculate the required exposure time. Fig. 3 shows such a micrograph of a *M. magnetotacticum* at an exposure time of 0.05 s. The signal-to-noise ratio (SNR) at the area of interest is 10, which is appropriate for elemental mapping. Under the same

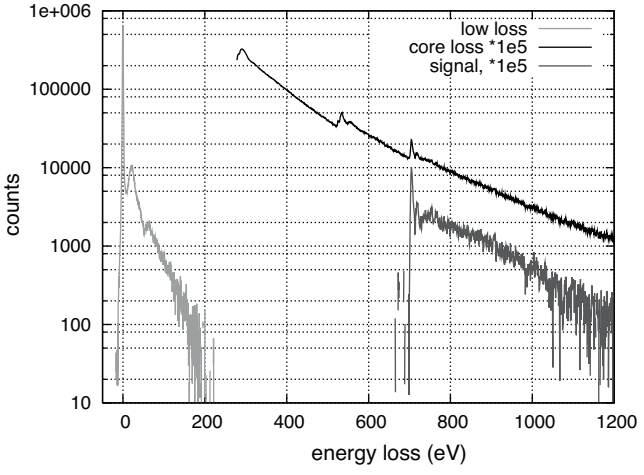

Fig. 2. EELS spectrum of a magnetite particle from *Magnetospirillum magnetotacticum*. The intensity of the iron edge is 10^7 times smaller than in the elastic peak.

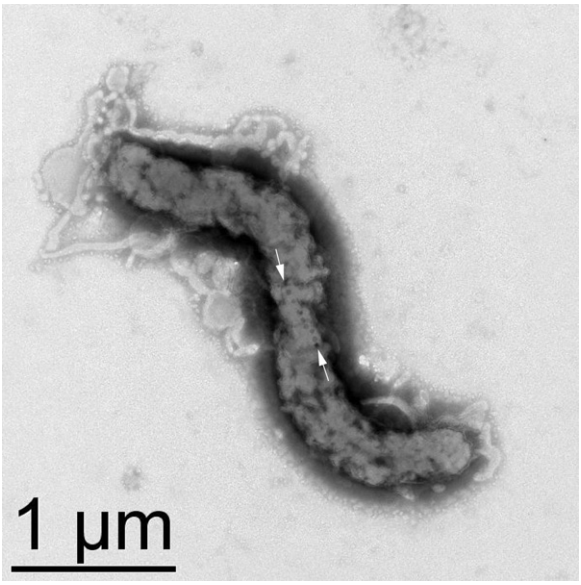

Fig. 3. Micrograph of the negatively stained *Magnetospirillum magnetotacticum* after being used for EMCD mapping. The row of magnetite particles is indicated with white arrows.

illumination conditions an exposure time of 5×10^6 s is required. For the elemental maps in the chiral positions the intensity was increased by 10^4 by reducing the beam diameter 100 times leading to an exposure time of 500 s per frame. Moreover, six frames are needed for the two elemental maps on both chiral positions. By this approach we were able to map an area of $120 \times 120\,\text{nm}^2$. The mechanical stability of the sample within the TEM and the resistivity against beam damage is still crucial for such an experiment. In the present case no beam damage was observed on the whole bacterium even after the long electron beam irradiation during the EMCD experiment (see Fig. 3). Additionally, the microscopy lab is located in a very stable environment, where mechanical vibrations are damped by the building itself in order to avoid sample drift. An active magnetic field compensation system is also installed to limit the influence of external dynamical magnetic fields.

3. Results

3.1. EMCD spectrometry

First we recorded EMCD spectra on selected crystals as shown in Fig. 4. To achieve this, the crystal was tilted into three beam case (3BC) conditions and the spectrometer entrance aperture was located at the Thales circle (see Fig. 1). The experimental conditions employed were as follows: parallel illumination of the specimen (which also reduces the electron dose rate that the specimen has to withstand), the collection angle was set to be 2.9 mrad, 10 s acquisition time at a spectrometer dispersion setting of 0.5 eV per channel. The used Bragg reflection was of a (1 1 3)-type. The dichroic signal, which is the difference between the two ELNES spectra, is in the range of 25% at the Fe-L_3 edge. This value can also be expected for the EMCD map.

3.2. EMCD mapping

Generally, for acquisition of EMCD maps an individual magnetite crystal was tilted into 3BC conditions. The objective aperture was inserted in the back focal plane of the objective lens in order to select the chiral transitions. As shown in Fig. 5, two of the four particles were in 3BC conditions with their systematic row axes nearly

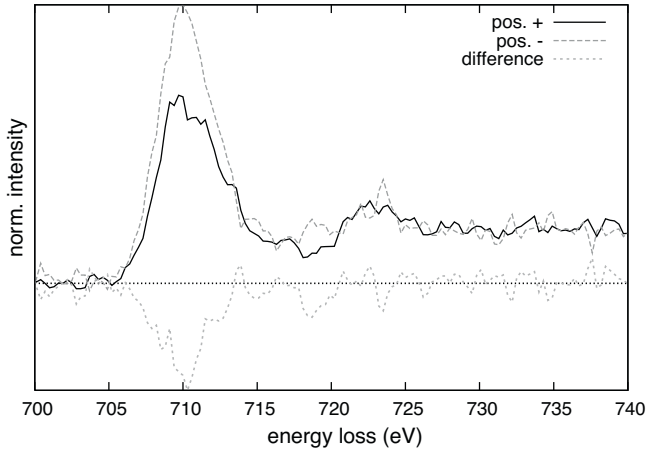

Fig. 4. Fe-$L_{2,3}$ ELNES after background subtraction recorded at the positions on the Thales circle as indicated in Fig. 1. The difference signal is the dichroic signal.

perpendicular to each other. Their Bragg reflections are called G_A, $-G_A$ being form the family of (1 1 3) reflections and G_B, $-G_B$ belonging to (2 2 0), respectively. Locating the OA on the right hand side, as indicated by the right circle in Fig. 5, gave a transition with positive chirality for the 3BC with index *A* and a transition with negative chirality for the 3BC indexed with *B*. For the left hand sided position of the OA the chiralities were opposing. Next we captured *inelastic dark field images* as shown in Fig. 6C and D. The dichroic map (or EMCD map) can then be calculated by

$$\frac{\Delta\sigma}{\sigma} = \frac{\sigma^+ - \sigma^-}{\sigma^+ + \sigma^-} \tag{3}$$

where σ^+ is represented by the elemental map from the position with positive chirality and σ^- is represented by the elemental map from the other position favoring transitions with negative chirality, respectively. Fig. 6 shows the experiment step-by-step: (A) the bright field image of the magnetic particles, (B) the dark field image, where only the $-G_A$ diffraction spot was chosen for imaging.

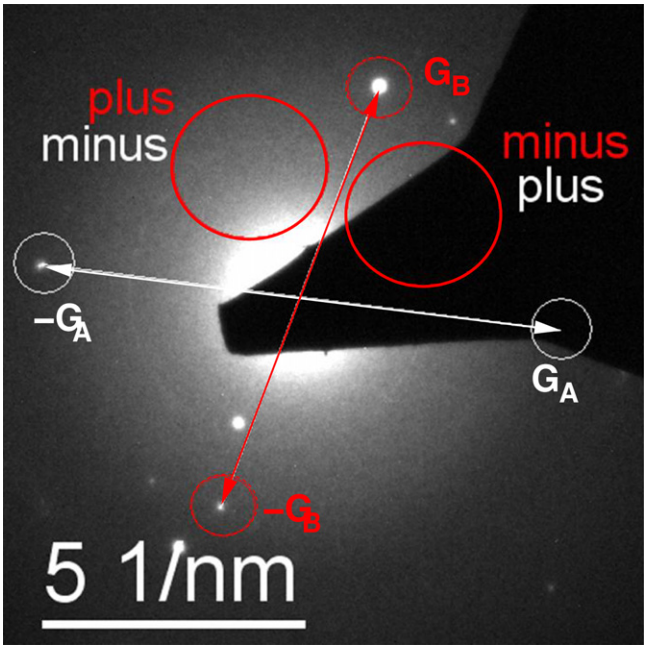

Fig. 5. Electron diffraction pattern of four magnetite particles. Two of them being in 3BC conditions, indexed with *A* and *B*. The OA positions are marked with large circles.

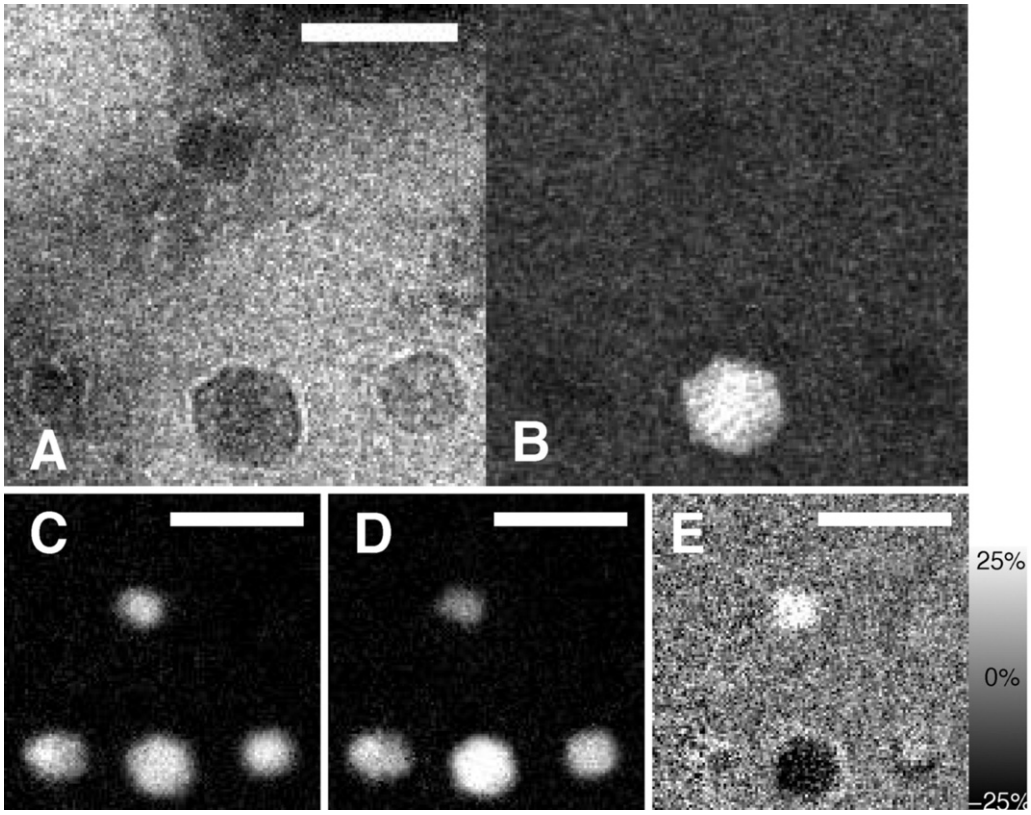

Fig. 6. (A) Bright field image of the magnetite particles. The white bar represents a distance of 50 nm. (B) Dark field image using the left most diffraction spot from Fig. 5. (C) Elemental map of iron L_3 using the left OA position. (D) Elemental map of iron L_3 using the right OA position as shown in Fig. 5. (E) Dichroic map.

In (C) and (D) the elemental maps of the Fe-L_3 edge are displayed by locating the OA at the chiral positions as indicated in Fig. 5. For the elemental maps the three window method was applied. The energy windows were located at 678 ± 7 eV, 694 ± 7 eV for the two background windows and 713 ± 7 eV for the Fe-L_3 edge window. Finally, the elemental maps from the two chiral positions were treated as described in Eq. (3), thus giving the final EMCD map (Fig. 6E).

3.3. Spatial resolution

Next we determined the spatial resolution of our experimental set up. In the present case the spatial resolution of the EMCD map can be measured simply by comparing the intensity profiles from the elastic dark field image (Fig. 6B) with the one from the EMCD map (Fig. 6E). The elastic dark field image was recorded with an exposure time of 3 s. Any drift would therefore be negligible when determining the particle size. Its diameter is found to be 32 nm (from the left to the right facet). For easier comparability the intensity profile from the EMCD map was inverted and normalized (Fig. 7). A quantitative comparison revealed that the mapped particle size is almost identical to the one in the quickly acquired dark field image. As the Coulomb delocalization for an energy loss of more than 700 eV is in the order of the extension of an 1s state it can be concluded that the sample drift is the limiting factor. Although the experiment was extremely stable, the sample drift can be estimated as being less than 3 pm per second.

3.4. Abiogenic magnetite

In order to determine whether or not the chemistry and crystal structure and therefore the ionicity of the iron ions on octahedral and tetrahedral crystal positions (Schattschneider et al., 2010) is comparable in biogenic and abiogenic magnetite, abiogenic crystals with a mean diameter of 7.9 ± 2.9 nm were also studied. To obtain a dichroic signal of a single Fe_3O_4 particle a convergent beam was used resulting in an illuminated sample area of approximately 5 nm in diameter. A nanocrystal oriented in 3BC was chosen for the measurement (right particle in Fig. 8A). The EELS spectra displayed in Fig. 8B were recorded using the set-up shown in Fig. 1 employing the SEA as the selection aperture for the chiral transitions. Comparison of the dichroic signal of the synthetized magnetite and the bio-mineralized magnetite with the simulations by Calmels and Rusz (2010) showing the thickness dependency of the EMCD signal indicates that the magnetic properties are not effected by the mechanism of mineralization.

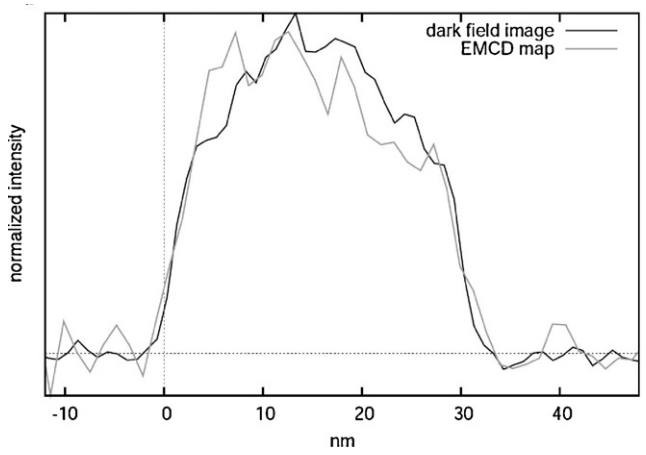

Fig. 7. Normalized intensity profiles of the dark field image and of the EMCD map from the particle being visible in the dark field image Fig. 6B.

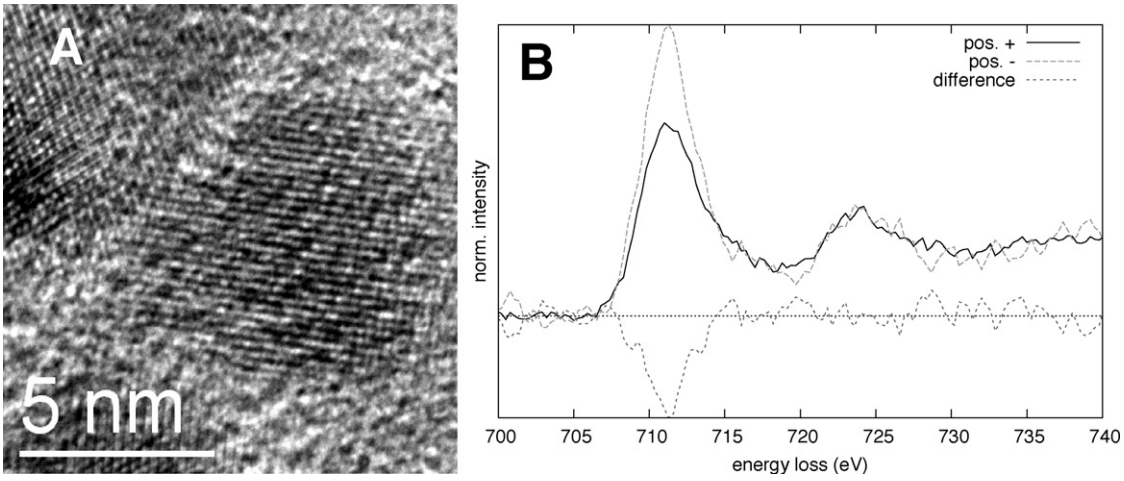

Fig. 8. (A) Magnetite nanoparticles and (B) the corresponding EELS spectra showing the transitions with positive and negative chirality and the EMCD signal (difference signal).

4. Discussion and outlook

In this paper we have reported the mapping of magnetic footprints with nanometer resolution in real space using EMCD. Although it is clear that the method needs to be developed further we have shown that EMCD can be employed as a complementary method to XMCD. Like the well established methods for investigating magnetism in the TEM, such as Lorentz microscopy and electron holography, EMCD will allow analysis of the magnetic properties of a specimen to a nm resolution. It has the potential for to be further developed to map atomic orbitals of magnetic materials in C_s-corrected TEMs.

The reader should be aware that the different contrast in the EMCD maps of Fig. 6E is not due to different magnetic behaviour of the particles but solely because of different illumination conditions. This means that one particle sees a right-handed illumination whereas the other one sees a left-handed illumination. This is a well known drawback of the *EMCD intrinsic way*, where the sample is used as a beam splitter and phase locker for the chirality experiment. If these grains would be investigated by means of XMCD, no different dichroic signature would be observed. To overcome this drawback a vortex beam could be used as recently suggested by Verbeeck et al. (2010): again no dichroic contrast would be visible. However, the EFTEM approach in combination with vortex beams is then limited to areas as small as the beam diameter, which is a few nanometers only.

Acknowledgements

The magnetite nanocrystals were provided by M.A. Neouze, Vienna University of Technology. The authors thank N. Fellner and M. Brandstetter for their support with electron microscopy at IMP-IMBA. M.S.-P. acknowledges the Hochschuljubiläumsstiftung of the municipality of Vienna, contract number H-01585/2007 for financial support. The work of G.P.R. was supported by the City of Vienna/Zentrum für Innovation und Technologie through the spot of excellence grant “Center of Molecular and Cellular Nanostructure”.

References

Batson, P.E., 1992. Spatial resolution in electron energy loss spectroscopy. Ultramicroscopy 47, 133–144.

Blakemore, R.P., 1975. Magnetotactic bacteria. Science 190, 377–379.

Calmels, L., Rusz, J., 2010. Momentum-resolved EELS and EMCD spectra from the atomic multiplet theory: application to magnetite. Ultramicroscopy 110, 1042–1045.

Dunin-Borkowski, R.E., McCartney, M.R., Frankel, R.B., Bazylinski, D.A., Posfai, M., Buseck, P.R., 1998. Magnetic microstructure of magnetotactic bacteria by electron holography. Science 282, 1868–1870.

Frankel, R.B., Blakemore, R.P., Wolfe, R.S., 1979. Magnetite in freshwater magnetotactic bacteria. Science 205, 1355–1356.

Gorby, Y.A., Beveridge, T.J.P.B.R., 1988. Characterization of the bacterial magnetosome membrane. J. Bacteriol. 170, 834–841.

Hébert, C., Schattschneider, P., 2003. A proposal for dichroic experiments in the electron microscope. Ultramicroscopy 96, 463–468.

Hébert, C., Schattschneider, P., Rubino, S., Novak, P., Rusz, J., Stöger-Pollach, M., 2008. Magnetic circular dichroism in electron energy loss spectrometry. Ultramicroscopy 108, 277–284.

Kohl, H., Rose, H., 1985. Theory of image formation by inelastically scattered electrons in the electron microscope. Adv. Electron. Electron Phys. 65, 172–227.

Jeanguillaume, C., Colliex, C., 1989. Spectrum image: the next step in EELS digital acquisition and processing. Ultramicroscopy 28, 252–257.

Krivanek, O., Dellby, N., Lupini, A.R., 1999. Towards sub-Å electron beams. Ultramicroscopy 78 (1–4), 1–11.

Lam, K.P., Hitchcock, A.P., Obst, M., Lawrence, J.R., Swerhone, G.D.W., Leppard, G.G., Tyliszczak, T., Karunakaran, C., Wang, J., Kaznatcheev, K., Bezylinski, D.A., Lins, U., 2010. Characterizing magnetism of individual magnetosomes by X-ray magnetic circular dichroism in a scanning transmission X-ray microscope. Chem. Geol. 270, 110–116.

Lidbaum, H., Rusz, J., Rubino, S., Liebig, A., Hjörvarsson, B., Oppeneer, P.M., Eriksson, O., Leifer, K., 2010. Reciprocal and real space maps for EMCD experiments. Ultramicroscopy 110, 1380–1389.

Löffler, S., Schattschneider, P., 2010. A software package for the simulation of energy-loss magnetic chiral dichroism. Ultramicroscopy 110, 831–835.

Maratea, D., Blakemore, R.P., 1981. Aquaspirillum magnetotacticum sp. nov., a magnetic spirillum. Int. J. Syst. Bacteriol. 31, 452–455.

Rose, H., 1999. Prospects for realizing a sub-Å sub-eV resolution EFTEM. Ultramicroscopy 78 (1–4), 13–25.

Rusz, J., Eriksson, O., Novak, P., Oppeneer, P.M., 2008. Spin and orbital momentum sum-rules for the electron energy-loss chiral magnetic dichroism. Phys. B: Condens. Matter 403 (5–9), 1614–1615.

Rusz, J., Rubino, S., Schattschneider, P., 2007. First-principles theory of chiral dichroism in electron microscopy applied to 3*d* ferromagnets. Phys. Rev. B 75, 214425.

Schattschneider, P., Ennen, I., Löffler, S., Stöger-Pollach, M., Verbeeck, J., 2010. Circular dichroism in the electron microscope: progress and applications. J. Appl. Phys. 107, 09D311.

Schattschneider, P., Rubino, S., Hébert, C., Rusz, J., Kunes, J., Novak, P., Carline, E., Fabrizionli, M., Panaccione, G., Rossi, G., 2006. Detection of magnetic circular dichroism using a transmission electron microscope. Nature 441, 486–488.

Schattschneider, P., Stöger-Pollach, M., Rubino, S., Sperl, M., Hurm, C., Zweck, J., Rusz, J., 2008. Detection of magnetic circular dichroism on the two-nanometer scale. Phys. Rev. B 78, 104413.

Verbeeck, J., Tian, H., Schattschneider, P., 2010. Production and application of electron vortex beams. Nature 467, 301–304.